International Journal of Mathematics and Computer Research

ISSN: 2320-7167

Volume 12 Issue 06 June 2024, Page no. – 4271-4275

Index Copernicus ICV: 57.55, Impact Factor: 8.316

DOI: 10.47191/ijmcr/v12i6.02

The Evolution of a Vivid Virtual the Cortex Avatar of Infant

Shubhangi D C[1], Baswaraj Gadgay[2], Maliha Mohammadi Begum[3]

[1]Department of Computer Science, Visvesvaraya Technological University CPGS Kalaburgi, Karnataka, India

[2]Department of Electronics and Communication, Visvesvaraya Technological University CPGS Kalaburgi, Karnataka, India

[3]Department of Computer Science, Visvesvaraya Technological University CPGS Kalaburgi, Karnataka,India

ARTICLE INFO

Published Online:
06 June 2024

Corresponding Author:
Shubhangi D C

ABSTRACT

In this paper, we present our process for developing digital cranial phantom for newborns that may be used to simulate MR images of the brain. Adult brain is foundation for several popular digital brain phantoms like BrainWeb. As more people become interested in using computer-aided methods for analyzing neonatal MR images, a demand for digital spectre & brain MR image simulator develops. This 3D digital brain phantom is comprised of 10 volumetric data sets which characterize spatial distribution of various tissues, having voxel intensity inversely correlated to amount of tissue contained inside the voxel. It is possible to simulate head tomography with help of digital brain phantom. This article discusses development of 3D digital infant neurocranial phantom & its application to the modeling of brain MR images.These pictures, with carefully orchestrated data deterioration, provide a typical, repeatable data set suitable for testing and training analytical techniques for neonatal MRI, such as segment & recognition algorithms.

KEYWORDS: Voxel, phantom, MR image, brain, skull, skin, fat ,memory, central nervous

I. INTRODUCTION

Ultra-high field (UHF), MRI devices are becoming more accessible, which is projected to greatly benefit broad aspects of uses in neurosciences. Most of essential functional & structural methods for brain imaging are based upon magnetic dependence, & UHF-MRI may enhance their sensitivity by increasing SNR & providing other specific enhancements in sensitivity. The improved sensitivity may therefore be exchanged freely for faster collection periods & finer spatial resolution, allowing for a far greater degree of specificity, even down to level of cortical columns & layers. Increased investment in developing more sophisticated UHF imaging methods and strengthening them to facilitate their trans0lation to ordinary clinical practice has resulted from the promised advantages of UHF-MRI & its expanding availability. Having access to a wide variety of theoretical & computational resources is crucial for making progress in this area. When considering latter, it becomes abundantly evident as robust computer modeling platforms are required, ones that are capable of accurately imitating biophysical properties and processes underpinning brain MRI, at high spatial resolution. Imaging simulations must take into account realistic distribution of such characteristics across the brain, but there are already well-established tools for simulating transformation of properties. To be more specific, there are two crucial prerequisites for a reliable simulating framework for high resolution (HR) brain MRI: 1. The need for complete brain coverage with accurate sub-millimeter-scale anatomical detail. Fractional volume impacts, sub voxel behavior, and motion can all be better modeled if spatial specificity is far higher than resolution limitations of imaging technology being studied. 2. many biophysical variables that influence the result of MR image acquisitions must be accounted for at this granular level. This entails characteristics of relaxation like T1, T2, & T2*, as well as impacts generated by susceptibility & B0 & B1 in homogeneities.

The aforementioned needs of simulation platform, or digital phantom, may be met in several ways. Long-duration UHF acquisitions have yielded a variety of publicly accessible fine-scale in-vivo MRI datasets with resolutions up to 100 µm. While some research has focused on high-resolution in-vivo data, others have looked at low-resolution data from a variety of modalities to define probability maps for different types of tissue. to enable more versatile simulations at moderate resolution in wide range of contrasts. Such methods do inherently provide accurate anatomical data for simulations,

including accurate MRI characteristics. They do, however, have significant drawbacks: (i) the achievable resolution is still limited by impractically long acquisition times necessitated by extra k-space readout stages and necessity for more averaging repeats to obtain a tolerable SNR; (ii), For a given anatomical sample, many publicly accessible datasets only represent a subset of whole range of MRI characteristics, particularly at higher resolutions, (iii) Artifacts (such as motion & breathing in-vivo, small air bubbles, & changing MR characteristics ex-vivo) may be decreased using specialized procedures, but they cannot be eliminated entirely, therefore acquisitions will always have some noise. (iv) utilizing parallel imaging methods to speed up acquisition process has risk of introducing biases that affect image's characteristics, which may throw off results of simulations. Many simulation phantoms were developed using just mathematical models, in contrast to actual brain records.

II. RELATED WORK

It is difficult to evaluate various segmentation methods without first knowing precise spatial distribution of brain tissues in MRI images [16]. No existing physical phantoms come close to meeting this criteria. Even most advanced digital brain phantoms come lacking as they cannot simulate precise structure & homogeneity of tissue as well as cannot manage independently anatomical regions (such as the basal ganglia). Here, we provide a software-based method for creating a lifelike MRI digital brain phantom. The phantom has data of 24x19x15.5cm volume of "normal" head in hydrogen nuclear MRI spin-lattice R1, spin-spin relaxation rate (R2), & PD. Phantom has 17 normal tissues that are distinguished by their own unique mean value & variances in R1, R2, & PD. Lesions caused by Multiple Sclerosis (MS) may also be replicated as a separate tissue type if desired. By simulating CSE & FFE procedures, MR pictures of brain were created on phantom. As an illustration of phantom's use, we give outcomes of mono-parametric segmentation performed on simulated sequences with varying levels of noise & slice thickness.

The grey matter, white matter, muscle, skin, and other tissues in aforementioned 3D digital brain phantom are defined by 10 volumetric data [17] sets, wherein voxel intensity proportional with percentage of tissue inside voxel. Digital phantom of brain may be utilized to replicate head tomography scans. Brain phantom is benchmark against which analytic methods, like classification processes, may be evaluated if they aim to determine tissue "type" of every image voxel.

In this study, our objective was to fulfill the requirement by creating an innovative digital representation with accurate anatomical intricacy [18], capable of achieving a resolution of up to 100µm. This digital phantom incorporates many MRI characteristics that influence the process of picture formation. Phantom known as BigBrain-MR was created by utilizing overtly accessible BigBrain histological dataset & low-resolution in-vivo 7T-MRI data. This was achieved through implementation of a novel image processing framework, which facilitated translation of overall characteristics of MRI data into detailed anatomical scale of histological dataset.

III. PROPOSED SYSTEM

The skin, fat, muscle, the dura mater, grey matter, & cerebrospinal fluid are only some of the nine tissue types which make up newborn brain phantom generated in the given research. Each voxel's vector consists of nine parts, each associated with nine tissue types. This digital phantom allows for visualization of the newborn skull in simulated MR images by integrating simulated magnetic resonance signal intensities. To facilitate the development and test of delineation & alignment algorithms for newborn MRI analysis, these images with controlled decrease of image quality offer typical, repeatable data set.

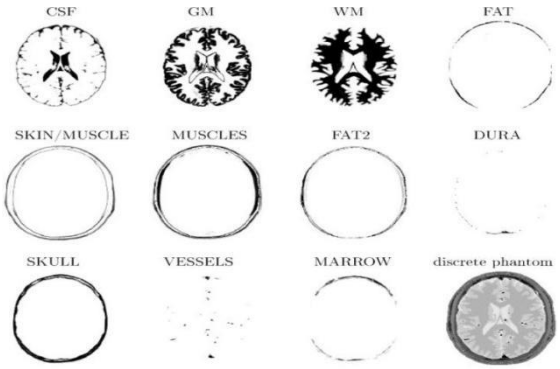

Figure 1: Nine Tissues

IV. METHODOLOGY

It is proposed to guide neonatal picture segmentation using specified atlas built from image obtained at later time-point of same subject. Our algorithm is made up of two parts: (1) The use of fuzzy logic to separate postmortem photos and create a probabilistic atlas of tissue The second stage is a combined registration & tissue segmentation of newborn picture using an atlas. Specifically, we executed atlas registration, & atlas-based tissue segmentation throughout combined registration & segmentation process. Tissue segmentation findings of photos taken at various ages, such as those taken at 1 and 2 years of age, may be utilized to inform segmentation of newborn images. In experiment section, we compare and offer information on their respective performances to assess the potential variation of newborn segmentation outcomes throughout time. To create a subject-specified atlas for neonatal segmentation, fuzzy segmentation method is used to later time-point picture of same subject in order to obtain tissue probabilistic maps of GM, WM, & CSF. By repeatedly calculating a mean intensity for every class & categorizing voxels in class with closest frequency centroid, K-means method segments an image. This is where fuzzy segmentation, comes from. Each voxel may include a mixture of GM, WM, & CSF because of the partial volume effect.

Fuzzy c-means (FCM) method accounts for this uncertainty by modeling voxel memberships. Each voxel's degree of class membership uncertainty is quantified by the membership metric. To pinpoint fuzzy membership functions & centroids c in a certain picture I, the typical FCM seeks to optimize following objective function:

$$\mathrm{EFCM}(\mu, c) = \sum_{j,k}^{n} \mu_{j,k}^{q} ||\mathrm{Ij} - \mathrm{ck}||^{x} \text{ ----- (1)}$$

wherein Ij is observed image intensity of voxel j in image domain, ck is centroid of class k, j,k is membership value of class k in voxel j, and q is weighted factor for every fuzzy membership that determines degree of fuzziness of resultant classification. In many contexts, value 2 is used for the q parameter. Intensity pattern of brain tissues & efficacy of fuzzy clustering may be affected by possibility of intensity inhomogeneity un MR images, but this is not something that may be handled by the typical FCM. AFCM method successfully addressed this issue by carrying out fuzzy clustering & intensity inhomogeneity assessment at the same time. To sum up, we need to find minimum value of following objective function:

$$E_{AFCM} = \sum_{j,k} \mu_{j,k}^{q} \|I_j - g_j c_k\|^{\mathbf{z}} + \lambda_1 \sum_{j,r} (D_r * g)_j^{\mathbf{z}} + \lambda_{\mathbf{z}} \sum_{j,r,s} (D_r * D_s * g)_j^{\mathbf{z}} \quad (2)$$

Where in gi is bias field in voxel j that is used to simulate intensity variation. In this research, finite difference operations along rth and sth picture dimensions, respectively, are denoted by Dr and Ds, respectively. For purpose of to ensure that bias field remains smooth and gradually varies, final two elements of equation (2) are 1st- & 2nd-order regularization terms. Picture histogram is estimated to get the centroids, which are then utilized to determine whether or not a given voxel belongs to a certain class. By calculating space-varying difference, an approximation of the bias field may be made. Here, we use AFCM technique to softly segment picture at late time point, & thereby get probabilistic maps for 3 tissues: white matter (WM), gray matter (GM), & cerebrospinal fluid (CSF). Starting values for CSF, GM, and WM's centroid ck are an equal interval from lowest to highest picture intensity, whereas gj is evenly set to 1 over whole image. When largest change in membership functions across all voxels among 2 iterations is less than defined threshold, segmentation converges by repeatedly upgrading centroids & bias field. In Fig. 2, we see the iterative process's typical tissue segmentation result from an image that is two years old. It's important to note that the aforementioned procedures also provide 3 tissue probability maps for GM, WM, & CSF, which may be utilized as a subject-specific tissue probability atlas to direct newborn brain picture segmentation, as explained below.

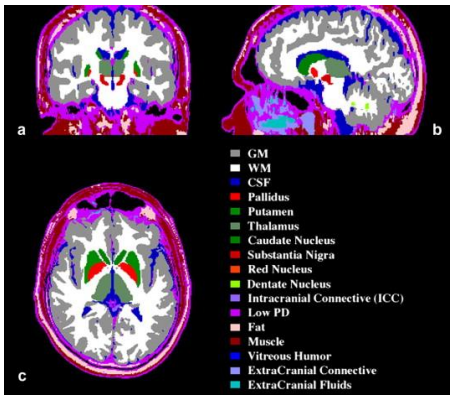

Fig-2: MRI digital brain phantom for validating of segmentation approaches

Image segmentation may be affected by the level of sharpness of atlas used. For instance, a weak atlas lacks adequate prior data that typically leads to loss of details in tissue segmentation results, whereas strong atlas relies more on atlas as well as produces results similar to the atlas. In this study, we utilise word "sharpness" to express the comparable effect on segmentation using individual atlases, while shifting balance amongst individual atlases (looking sharp) &an evenly distributed prior. We add a parameter t to adjust the relative importance of segmentation accuracy and atlas sharpness in following ways:

$$p_{j,k}^{new} = \frac{1-t}{K} + t * p_{j,k} \quad (3)$$

wherein K is number of brain tissues (K = 3 in this research), pnewj,k is adjusted tissue probability j(∑kpj,k=1), and pj,k is probabilities of tissue class k in a particular voxel j. The first version of sharp individualized atlas is utilized whenever t = 1. When time is zero, this uniform global prior is applied to all tissue probabilities. The efficiency of tissue segmentation may be improved by adjusting the proportion of longitudinal information utilized as a guide by improving parameter t. In the experiment section, we will go further into these t value ranges.

K-Means Algorithm

Algorithm work is elaborated as:

1 We begin by picking k sites at random to serve as averages or cluster hubs.

2 Every object is placed in cluster with mean value closest to it, & coordinates of mean are updated based on the new averages of objects placed within this cluster.

3 We repeat the procedure till we have desired number of clusters.

The "points" discussed above are termed means because they represent average values of objects placed in their respective categories. There are a variety of ways we may get started with these resources. The means may be intuitively initialized by selecting data points at random. Means may also be initialized using random values within range of dataset (for

example, if items for feature x have values among 0 and three, means shall be set to 0 and 3).

Here is above algorithm written in pseudocode:

Initialize k means with random values

--> For a given number of iterations:

--> Iterate through items:

--> Find the mean closest to the item by calculating the Euclidean distance of the item with each of the means

--> Assign item to mean

--> Update mean by shifting it to the average of the items in that cluster

V. SYSTEM ARCHITECTURE

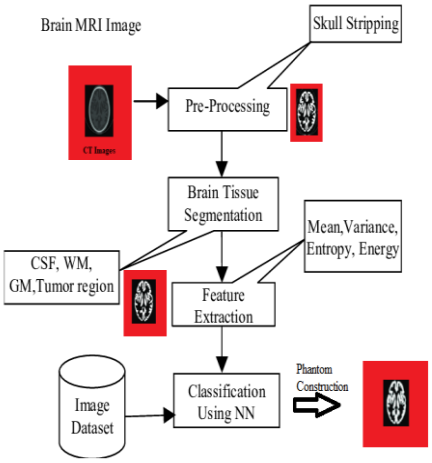

Fig-3: System Architecture

Brain picture input undergoes preprocessing to eliminate noise and convert to gray scale, after which it is segmented into several areas, features are extracted, classification is carried out, & 3D brain image is produced.

VI. RESULT AND DISCUSSION

The main singular traits have to be differentiated from other further or undesirable data in order to improve image quality in order that we may evaluate it more efficiently. Segmented images are those which have undergone additional preprocessing and splitting in multiple parts. In the previous research, an adult's 3D brain structure was provided; in the current study, a one-year-old's brain is provided in 3D.

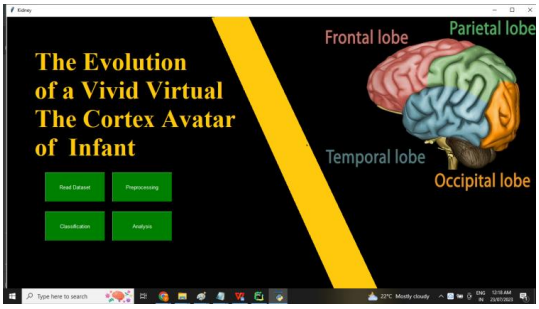

Fig-4:Menu

This is menu application that we may use to carry out steps.

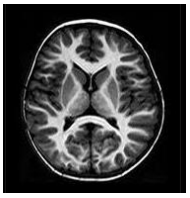

Fig-5: Read Image

Its utilised for selecting input image

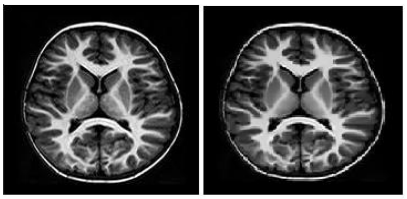

Fig-6: Enhancing image's quality beforehand allows for more precise analysis. Preprocessing lets us get rid of artifacts & boost attributes which are important most for use case.

Fig-7: Segmented Image

partitioning image in several parts, commonly depends upon an image's pixel properties

Fig-8: Feature Extraction

part of pattern recognition when irrelevant data is filtered out & core signal properties are isolated.

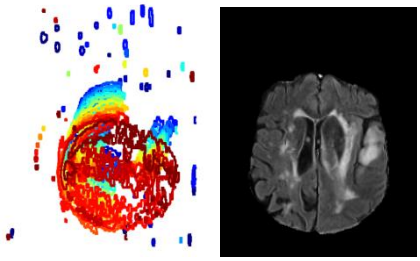

Figure 8: 3D Brain Construction

Output of 1 year baby 3d Brain image

VII. CONCLUSION

In order to better understand how to tune, test, & compare segmentation algorithms, digital MRI brain phantom and

acquisition simulation technique have been developed. When evaluating effectiveness of segmentation strategies, our digital phantom has many benefits over existing options.

REFERENCES

1. P. Hemler, P. van den Elsen, T. Sumanaweera, S. Napel, J. Drace, and J. Adler, "A quantitative comparison of residual error for three different multimodality registration techniques," in Information Processing in Medical Imaging, Y. Bizais and C. Barillot, Eds. Ile Berder, France: IPMI, Kluwer, 1995, pp. 251–262.
2. J. C. Rajapakse, C. DeCarli, A. McLaughlin, J. N. Giedd, A. L. Krain, S. D. Hamburger, and J. L. Rapoport, "Cerebral magnetic resonance image segmentation using data fusion," J. Comput. Assist. Tomogr., vol. 20, pp. 206–18, Mar./Apr. 1996.
3. E. Hoffman, P. Cutler, W. Digby, and J. Mazziotta, "3-D phantom to simulate cerebral blood flflow and metabolic images for PET," IEEE Trans. Nucl. Sci., vol. 37, pp. 616–620, 1990.
4. E. Hoffman, P. Cutler, T. Guerrero, W. Digby, and J. Mazziotta, "Assessment of accuracy of PET utilizing a 3-D phantom to simulate the activity distribution of FDG uptake in the human brain," J. Cereb. Blood Flow Metab., vol. 11, pp. A17–A25, 1991.
5. H. J. Kim, J. S. Karp, P. D. Mozley, S. O. Yang, D. H. Moon, H. F. Kung, H. K. Lee, and A. Alavi, "Stimulating technetium-99 m cerebral perfusion studies with a threedimensional Hoffmann brain phantom:4http://www.bic.mni.mcgill.ca/brainweb. Collimator and fifilter selection in SPECT neuroimaging," Ann. Nucl. Med., vol. 10, pp. 153–160, Feb. 1996.
6. S. Eberl, I. Kanno, R. R. Fulton, A. Ryan, B. F. Hutton, and M. J. Fulham, "Automated interstudy image registration technique for SPECT and pet," J. Nucl. Med., vol. 37, pp. 137–45, Jan. 1996.
7. J. Li, R. J. Jaszczak, and R. E. Coleman, "A fifiltered backprojection algorithm for axial head motion correction in fan-beam SPECT," Phy. Med., Biol., vol. 40, pp. 2053–2063, Dec. 1995.
8. D. Mahoney, S. Huang, A. Ricci, J. Mazziotta, R. Carson, E. Hoffman, and M. Phelps, "A realistic computer-simulated brain phantom for evaluation of PET characteristics," IEEE Trans. Med. Imag., vol. MI-6, pp. 250–257, 1987.
9. H.-J. Kim, B. Zeeberg, F. Fahey, A. Bice, E. Hoffman, and R. Reba, "3-D SPECT simulations of a complex 3-D mathematical brain model and measurements of the 3-D physical brain phantom," J. Nucl. Med., vol. 32, pp. 1923–1930, 1991.
10. Y. Narita, H. Iida, B. A. Ardekani, J. Hatazawa, I. Kanno, T. Nakamura, and K. Uemura, "Evaluation of partial volume effect in quantitative measurement of regional cerebral blood flflow using positron emission tomography," (in Japanese) Kaku Igaku—Jpn. J. Nucl. Med., vol. 32, pp. 163–72, Feb. 1995.
11. H. Iida, Y. Narita, B. A. Ardekani, J. Hatazawa, M. Nakazawa, I. Kanno, and K. Uemura, "Evaluation of partial volume effect in quantitative measurement of regional cerebral blood flflow in single photon emission computed tomography-effects of limited spatial resolution and fifirst pass extraction fraction," Kaku Igaku—Jpn. J. Nucl. Med., vol.32, pp. 155–62, Feb. 1995.
12. D. Collins, C. Holmes, T. Peters, and A. Evans, "Automatic 3-D modelbased neuroanatomical segmentation," Human Brain Mapping, vol. 3, no. 3, pp. 190–208, 1995.
13. Y. Ma, M. Kamber, and A. C. Evans, "3-D simulation of PET brain images using segmented MRI data and positron tomograph characteristics," Computerized Med. Imag., Graphics, vol. 17, pp. 365–371, July/Oct. 1993.
14. R. Kwan, A. C. Evans, and G. B. Pike, "An extensible MRI simulator for post-processing evaluation," in Proc. 4th Int. Conf. Visualization in Biomedical Computing, VBC '96, Hamburg, Sept. 1996, pp. 135–140.
15. C. Holmes, R. Hoge, D. Collins, R. Woods, A. Toga, and A. Evans, "Enhancement of MR images using registration for signal averaging," J. Comput. Assist. Tomogr., vol. 22, pp. 324–333, Mar. 1998.
16. Bruno Alfano, Gioacchino Tedeschi , Arturo Brunetti, MarSalvatore ,2011, "An MRI digital brain phantom for validation of segmentation methods"
17. Design and construction of a realistic digital brain phantom D. L. Collins1, Alex P. Zijdenbos2, V. Kollokian2 +4 more•Institutions (2) 01 Jun 1998- IEEE Transactions on Medical Imaging (IEEE)-Vol. 17, Iss: 3, pp 463-468
18. BigBrain-MR: a new digital phantom with anatomically-realistic magnetic resonance properties at 100-µm resolution for magnetic resonance methods development Cristina Sainz Martinez,1,2 Meritxell Bach Cuadra,2,3 João Jorge 1,2022,